



## Evaluating the Microstructure and Strength of Geopolymer Mud Blocks for Sustainable Architecture

A. Kandasamy<sup>1\*</sup>, B. Ramesh<sup>1</sup>, Mahmoud Al Khazaleh<sup>2</sup>, K. Sabari<sup>3</sup>

<sup>1</sup> Department of Civil Engineering, Saveetha School of Engineering, Saveetha Institute of Medical and Technical Sciences, Chennai, Tamil Nadu, 602105, India.

<sup>2</sup> Department of Civil Engineering, Munib and Angela Masri Faculty of Engineering, Aqaba University of Technology, Aqaba, 11947, Jordan.

<sup>3</sup> Department of Mechanical Engineering, Saveetha School of Engineering, Saveetha Institute of Medical and Technical Sciences, Chennai, Tamil Nadu, 602105, India.

Received 01 February 2025; Revised 17 March 2025; Accepted 22 March 2025; Published 01 April 2025

### Abstract

This study investigates the physio-mechanical, microstructural, and durability characteristics of Geopolymer Mud Blocks (GMB) as a sustainable alternative to traditional Soil Stabilized Blocks (SSB). Utilizing locally available Alumino-Silicate Sources (ASS) and Alkali-Activated Materials (AAM), GMB were produced with varying molarity levels (6M, 7M, and 8M) and mix proportions (M1 to M3). Experimental results reveal that compressive strength increased by 10–20% with molarity escalation from 6M to 8M. The highest compressive strength of over 50 MPa, achieved with the M4 mix at 8M, equaled M50-grade concrete, making it suitable for load-bearing walls in earthquake-resistant structures. Durability tests demonstrated less than 10% water absorption, indicating low permeability. Type B6 (6% AAS, 8M, 28 days) exhibited superior performance, attaining the highest compressive strength of 47.32 MPa and prism strength of 33.12 MPa. Additionally, it showed commendable durability metrics, including water absorption at 5.20%, chloride diffusion at 1.87%, acid diffusion at 3.33%, and sulphate diffusion at 1.05%. The dense matrix and minimal porosity of this mix, resulting from the use of distilled water and optimal binder content, significantly enhanced its strength and durability. Type C6 (6% AAS, 8M, 28 days) exhibited the weakest performance, characterized by high porosity, suboptimal matrix quality, and unfavorable durability indicators, such as water absorption (10.33%) and chloride diffusion (4.47%). Type B6 demonstrates the highest effectiveness, providing an optimal balance of strength and durability, whereas Type C6 exhibits the lowest efficiency. GMB exhibited enhanced resistance to acid, sulphate, and chloride attacks with increased molarity. XRD analysis confirmed the geopolymerization process, with significant diffraction peak changes. SEM images revealed denser microstructures with higher molarity, correlating with increased strength. The study concludes that GMBs offer superior strength, durability, and cost-strength efficiency compared to SSBs, promoting sustainable construction practices.

**Keywords:** Geopolymer Mud Blocks (GMB); Soil Stabilized Blocks (SSB); Alumino-Silicate Sources (ASS); Alkali-Activated Materials (AAM); Durability Tests.

### 1. Introduction

The growing demand for sustainable construction materials has led to the exploration of alternative building materials that minimize environmental impact while maintaining structural integrity. Traditional construction materials, such as concrete and fired bricks, contribute significantly to greenhouse gas emissions and environmental degradation. One such promising alternative is the geopolymer mud block, which integrates geopolymer with traditional mud-based construction techniques to enhance strength, durability, and sustainability.

\* Corresponding author: [kandasamy9032.sse@saveetha.com](mailto:kandasamy9032.sse@saveetha.com)

 <http://dx.doi.org/10.28991/CEJ-2025-011-04-09>



© 2025 by the authors. Licensee C.E.J, Tehran, Iran. This article is an open access article distributed under the terms and conditions of the Creative Commons Attribution (CC-BY) license (<http://creativecommons.org/licenses/by/4.0/>).

Synthesized employing alkali activation of alumino-silicate minerals including fly ash and metakaolin, geopolymers have shown better mechanical and durability than traditional cement-based products [1, 2]. Excellent binding qualities, fast-setting periods, and increased resistance to chemical assault define these materials. By using industrial and agricultural waste products such as fly ash, rice husk ash, and slag in the formulation of geopolymers binders, their sustainability profile is further improved and landfill trash and the carbon footprint of building projects are decreased [3, 4]. Recent developments show that using recycled materials in geopolymer composites not only enhances mechanical qualities but also helps environmental preservation by lowering carbon emissions and trash creation [5, 6].

Mud blocks have been recognized for their energy efficiency, low embodied carbon, and flexibility to local climatic conditions [7, 8]. Mud blocks are a sustainable option, unlike traditional burnt bricks, which need high-temperature kilns and help to contribute to deforestation using little processing of natural resources. But their mechanical characteristics, especially compressive strength and durability, often restrict their general acceptance in structural use [9, 10]. To address these limitations, investigators have explored various steadiness techniques, including the use of cement, lime, and natural fibers [11, 12]. Although these techniques boost strength, their embodied energy and carbon footprint usually suffer. Using geopolymers as a stabilizing ingredient offers a fresh technique that greatly increases the compressive strength, water resistance, and lifetime of mud blocks without requiring energy-intensive processing [13, 14].

Determination of the performance of geopolymer mud blocks depends critically on their microstructural properties. The reaction processes of geopolymerization produce a dense and compact matrix, therefore lowering porosity and improving mechanical characteristics. Energy Dispersive Spectroscopy (EDS) and Scanning Electron Microscopy (SEM) studies provide an understanding of the shape, porosity, and elemental makeup of geopolymer matrices, thereby guiding material compositions for maximum mechanical performance and durability [15, 16]. Moreover, the actual use of these blocks in sustainable buildings depends on an awareness of their long-term stability under the influence of environmental elements like CO<sub>2</sub> exposure, water absorption, and moisture intrusion [17, 18].

Recent studies have shown how different aggregates and fiber reinforcement help to increase the strength and durability of geopolymer mud blocks. Investigated for their ability to improve flexural strength and lower brittleness are natural fibers such as coir, hemp, and sisal [19, 20]. To improve the practical usage of these materials, also investigated are the effects of chemical composition, curing conditions, and environmental factor exposure. Appropriate for many climatic settings, optimized geopolymer formulations have demonstrated enhanced resilience to weathering, sulfate attack, and freeze-thaw cycles [21, 22].

This study aims to bridge these gaps by systematically evaluating the mechanical and durability properties of GMBs with varying AAM molarity levels. The findings will contribute to optimizing geopolymer formulations for sustainable and cost-effective construction, particularly in regions with abundant red soil resources. From the preceding literature, nobody takes into account varying molarity levels and the creation of AAM using geopolymer mud blocks. Incorporating studies of mechanical strength, microstructural properties, and durability assessments, this work offers a fresh approach to maximizing geopolymer mud blocks. This work methodically investigates AAM type, concentration, molarity, and water purity, therefore providing fresh scientific ideas and useful advice for the creation of environmentally friendly, high-performance masonry materials. The results show significant progress in tying laboratory research with useful building purposes together.

## 2. Materials and Methods

Table 1 demonstrates the chemical makeup of the basic components. High in alumina ( $Al_2O_3$ ) and iron oxide ( $Fe_2O_6$ ), red soil is a naturally occurring soil with a characteristic red or reddish-brown color. Essential in polymerization, this component supplies the alumina needed for the chemical process and the reactive silica ( $SiO_2$ ). With a bulk density of around 1.8 g/cm<sup>3</sup>, red soil is distinguished by its clayey texture, modest flexibility, and low porosity. With little organic content, the composition—silica, alumina, and iron oxide—makes sense for industrial applications like the manufacture of geopolymer. M-Sand Designed to replace natural river sand in building uses, manufactured sand—also known as M-sand—is a fine aggregate produced by crushing hard stones. Along with small amounts of feldspar and mica, the composition mostly consists of silica ( $SiO_2$ ) as quartz. With grain sizes ranging from 0.075 to 4.75 mm, M-sand has a well-graded distribution marked by angular particles enhancing interlocking within the geopolymer mixture.

Maintaining regulated moisture content and a bulk density between 1.75 and 1.95 g/cm<sup>3</sup>, the material shows dependability and durability for use in geopolymer. Made as a by-product of coal burning in thermal power plants, fly ash is a fine, grey powder. High silica ( $SiO_2$ ) and alumina ( $Al_2$ ) compositions define the work; 50–60% and 20–30%, respectively. Trace levels of magnesium oxide (MgO), lime (CaO), and iron oxide ( $Fe_2O_3$ ) also are present. Usually measuring less than 75 μm in diameter, fly ash particles have a spherical form and fine texture; their specific gravity falls between 2.1 and 2.6. Crucially important in geopolymerization, this substance shows pozzolanic activity by interacting with alkalis to generate cementitious compounds. A by-product of iron manufacture in blast furnaces, ground

granulated blast furnace slag (GGBS) is much sought after as additional cementitious material. In approximate terms, the composition calls for calcium oxide (CaO), silica (SiO<sub>2</sub>), alumina (Al<sub>2</sub>O<sub>3</sub>), and magnesium oxide (MgO) in 30–50%, 30–40%, 7–16%, and 8–12%, respectively. GGBS is a fine powder characterized by a pale grey hue, a specific gravity ranging from 2.8 to 3.0, and a high Blaine fineness of 400 to 500 m<sup>2</sup>/kg. The latent hydraulic reactivity, which is activated by alkalis, renders it highly effective for enhancing the mechanical properties of geopolymer. Sodium hydroxide (NaOH) is a highly caustic metallic base and alkali salt. It is commonly used in various industrial processes, including the manufacture of soap, paper, and textiles, as well as in water treatment and chemical synthesis [23]. Figure 1 illustrates the workflow, which briefly shows the process of the methodology.

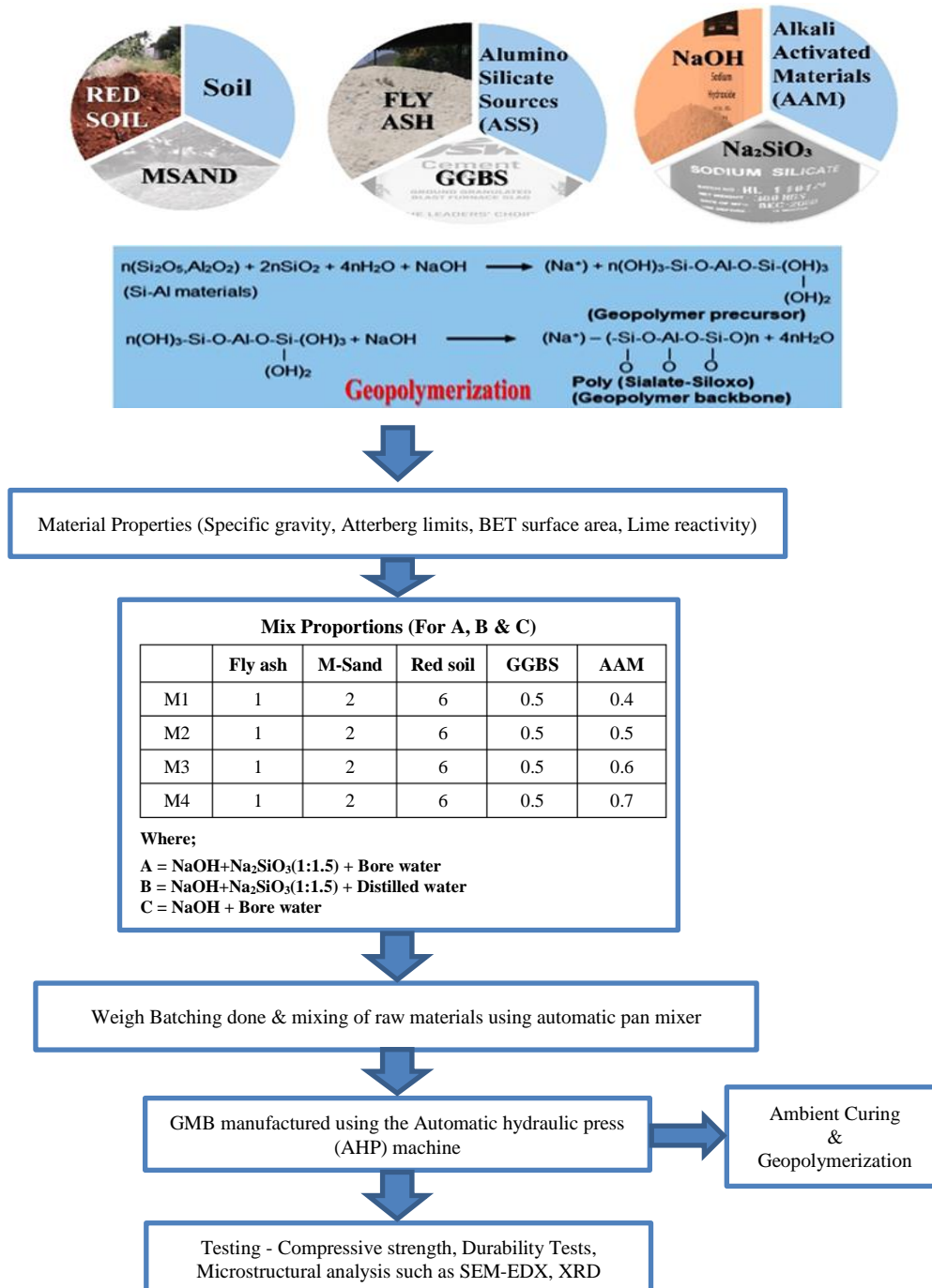


Figure 1. Methodology of the work

The particle size distribution curve (Figure 2) of the red soil shows that it contains a clay-size fraction around 42% (<2 mm), 12% silt, and 45% sand. The particle size distribution curves of GGBS and fly ash are shown in Figure 2. The grain size curves show that GGBS has a 1.75% sand-size fraction, 85.59% silt-size fraction, and 7.95% clay-size fraction, whereas fly ash consists of a 17.9% sand-size fraction, 72.39% silt-size fraction, and 7.25% clay-size fraction.

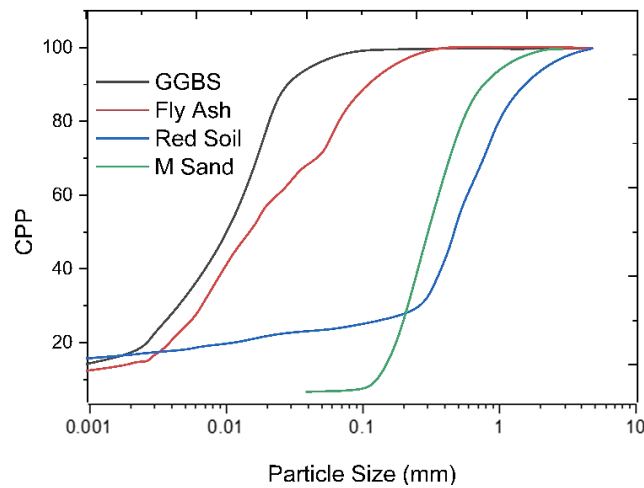


Figure 2. Grain size distribution curve for materials used in GMB

Sodium hydroxide (NaOH) is a potent alkali that functions as an activator in the process of polymerization. This substance is a white crystalline solid characterized by a high pH of approximately 14 and exhibits significant reactivity with water, resulting in heat release upon dissolution. The process involves the dissolution of silica and alumina from the raw materials, thereby initiating the polymerization reaction. Sodium hydroxide (NaOH) exhibits a melting point of 318°C, a density of approximately 2.13 g/cm<sup>3</sup>, and demonstrates high solubility in water, thereby enhancing its function as a catalyst in the synthesis of the geopolymer precursor. Comprising sodium, silicon, and oxygen, sodium silicate, with the chemical formula Na<sub>2</sub>SiO<sub>3</sub>, is a compound. Commonly known as water glass, sodium silicate is a binder used in polymerization [24, 25]. Reactive silica (SiO<sub>2</sub>) and sodium oxide (Na<sub>2</sub>) help the geopolymer network to grow. It occurs as a translucent, viscous liquid or in solid form; while liquid, its density is 1.4–1.6 g/cm<sup>3</sup>. Complete solubility in water and alkaline properties make sodium silicate a vital component for increasing the strength and lifetime of geopolymers. A vital part of polymerization, water serves as a solvent for sodium hydroxide and sodium silicate. This procedure helps to dissolve aluminosilicate sources and accelerates the required chemical processes to build the geopolymer framework. It is chemically neutral, exhibiting a pH of 7, and possesses a density of approximately 1 g/cm<sup>3</sup> at room temperature. Water plays a vital role in maintaining the appropriate consistency and reactivity of the geopolymer mixture. Figure 3 illustrates the manual mixing of the GPMB [26, 27]. Figures 4 and 5 illustrate the base products of AAS and AAM. In our study, we also use distilled water for comparison with water. The use of distilled water in the polymerization process helps eliminate impurities, such as dissolved salts and organic matter, which may interfere with the reaction between the ASS and the AAM. Impurities in regular water can affect the setting time, strength development, and overall consistency of the geopolymer matrix. By using distilled water, we ensured better control over the reaction kinetics and reproducibility of the results.

Table 1. Chemical Composition of Base Materials of Bricks.

Material	SiO <sub>2</sub> (%)	Al <sub>2</sub> O <sub>3</sub> (%)	Fe <sub>2</sub> O <sub>3</sub> (%)	CaO (%)	MgO (%)	Na <sub>2</sub> O + K <sub>2</sub> O (%)	SO <sub>3</sub> (%)	Other Components (%)
Red Soil	55	25	12	3	2	1.5	0.5	1.0 (Organic matter, moisture)
M-Sand (Manufactured Sand)	75	8	3	1.5	0.5	0.8	0.2	1.0 (Trace impurities)
Fly Ash (Class F)	55	25	7	3	1.5	1.5	2	5 (Loss on ignition)
Ground Granulated Blast Furnace Slag (GGBS)	35	12	1.5	40	8	1.5	1.5	1 (Trace elements, LOI)

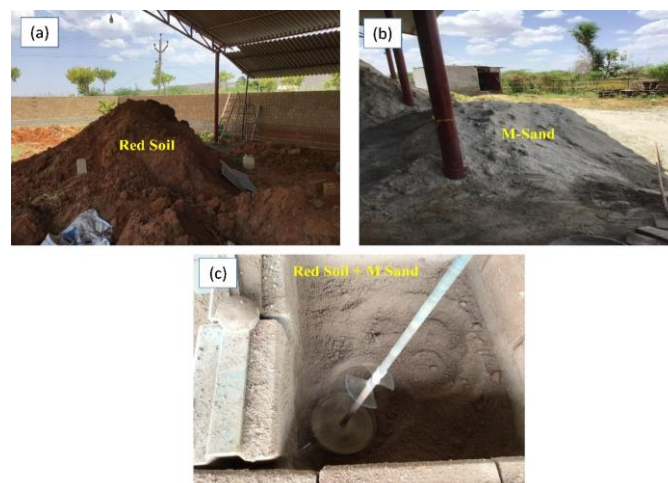
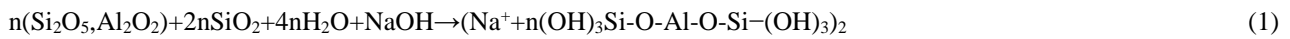


Figure 3. Manual mixing of Red Soil and M-Sand.



Equations 1 and 2 clearly explain the formation of geopolymer. The geopolymerization process comprises two fundamental reactions. Initially, aluminosilicate materials ( $\text{Si}_2\text{O}_5$ ,  $\text{Al}_2\text{O}_2\text{Si}_2\text{O}_5$ ,  $\text{Al}_2\text{O}_2$ ) dissolve in sodium hydroxide (NaOH), water ( $\text{H}_2\text{O}$ ), and additional silica ( $\text{SiO}_2$ ), resulting in the formation of sodium-stabilized oligomers ( $(\text{OH})_3\text{Si-O-Al-O-Si-(OH)}_3$ ), known as the geopolymer precursor. This step disaggregates the raw materials into reactive units. In the subsequent step, these oligomers participate in a condensation reaction facilitated by sodium hydroxide, resulting in the formation of a three-dimensional poly (sialate-siloxo) network ( $(-\text{Si-O-Al-O-Si-O})_n$ ). The polymerization process results in the formation of a stable geopolymer structure, accompanied by the release of water as a by-product. These reactions convert raw aluminosilicate sources into a durable polymeric material [28].

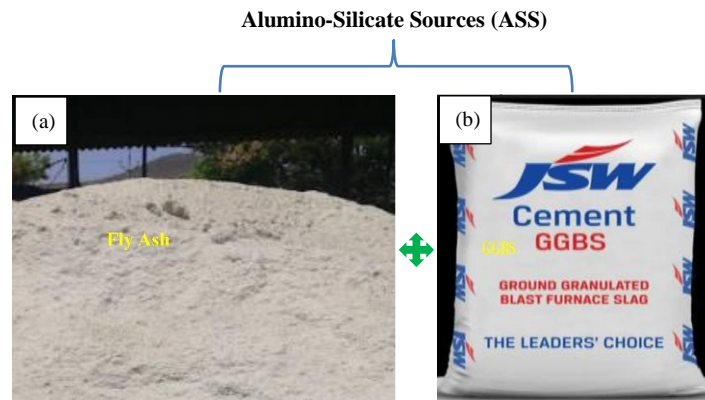


Figure 4. Aluminosilicate Sources (ASS)



Figure 5. Making of AAM

Table 2 illustrates the preparation of bricks utilizing the designated materials and Alkali Activator Solutions (AAS), which entails meticulous material preparation, mixing, molding, and curing processes. The composition consists of 60% red soil, 20% fly ash, 5% Ground Granulated Blast Furnace Slag (GGBS), and 10% M. Sand, along with the suitable Alkali Activator Solution. The composition of the Alkali Activator Solution is contingent upon its specific type. The solution for Type A consists of Sodium Hydroxide (NaOH) and Sodium Silicate ( $\text{Na}_2\text{SiO}_3$ ) in a 1:1.5 ratio, combined with bore water. NaOH pellets are dissolved in bore water to obtain the desired molarity, generally ranging from 6M to 8M, and subsequently combined with  $\text{Na}_2\text{SiO}_3$  in the specified ratio. The solution is agitated until homogeneous and permitted to cool before application. For Type B, the preparation is the same, with distilled water substituting bore water. The solution for Type C consists solely of NaOH dissolved in bore water at the specified molarity. Upon preparation of the activator solution, the dry materials are mixed comprehensively to achieve uniform distribution. The curing process

exhibits minor variations based on the specific type of solution utilized [29]. Types A and B bricks undergo curing at ambient conditions for 24–48 hours to achieve the initial setting, followed by optional heat curing in an oven or steam chamber at temperatures ranging from 60 to 90°C to improve strength. Type C curing is done similarly, but the absence of sodium silicate could cause a slower rate of strength development. The bricks air-dry after curing to reach the best strength before testing or application. When handling NaOH and  $Na_2SiO_3$ , one should follow safety measures, including wearing gloves and goggles. To guarantee consistency, the molarity of the NaOH solution has to be constant across batches; hence, the moisture content in the mixture should be ideal for both workability and strength. This methodical approach ensures the manufacturing of uniform-characteristic, high-quality bricks. Figure 6 shows the brick-making process using various NaOH molar concentrations [30].

**Table 2. Combinations of Alkali Activator Solutions (AAS)**

S.No	Alkali activator solution type	Compositions
1	A	NaOH + $Na_2SiO_3$ (1:1.5) + Bore water
2	B	NaOH + $Na_2SiO_3$ (1:1.5) + Distilled water
3	C	NaOH + Bore water



**Figure 6. Process of Making the Bricks with Different Molar of NaOH**

Using a traditional mix where cement replaces the Alkali Activator Solution (AAS), the brick preparation calls for using similar raw material ratios and mostly uses cement as the binding agent. With cement acting as the binder, the makeup calls for 60% red soil, 20% fly ash, 5% Ground Granulated Blast Furnace Slag (GGBS), and 10% manufactured sand. To get the mix ready, the dry components are first measured and weighed in line with the given ratios. Carefully mixed to guarantee consistency are red soil, fly ash, GGBS, and M. Sand. After that, cement is added to the dry mix; usually making 10% of the overall mix weight, this percentage may vary depending on the brick's needed strength and durability. Water is gradually added to get the desired consistency after the dry components have been mixed. The water content must be precisely regulated to prevent an excessively wet or dry mixture, thereby ensuring optimal workability and preserving the strength characteristics of the mix. The wet mixture is blended until a homogeneous consistency is attained. The prepared mixture is subsequently placed into brick molds and compacted with a hydraulic press to achieve uniform shape and density. After molding, the bricks are allowed to cure. In traditional cement-based brick production, the curing process generally requires maintaining the bricks in a moist environment or applying water to them for a duration of 7 to 28 days [31]. This facilitates adequate hydration of the cement, and the subsequent development of strength and size of the block is 225×115×70 mm.

### 3. Results and Discussion

#### 3.1. Mechanical Properties

##### Compressive Strength

Figure 7 illustrates the Compression Testing Machine (CTM) alongside the bricks utilized for experimental testing. The research examined bricks with different molarities and various samples to assess their compressive strength. The experiment was conducted in the laboratory of Saveetha School of Engineering (Chennai, India). Table 3 compares compressive strength (CS) values of bricks subjected to different Alkali Activator Solutions (AAS) and molarities (6M, 7M, and 8M) across curing periods of 7, 14, and 28 days. The conventional cement-based mix demonstrates compressive strength values of 4.6 MPa, 6.1 MPa, and 7.8 MPa for identical durations across all molarities shown in Figure 8. Figures 9 to 11 illustrate in detail that the AAS-based mixtures exhibit markedly elevated compressive strengths, with values contingent upon the solution type, AAS percentage, and molarity. The maximum compressive strength (CS) recorded was 47.32 MPa for Type B alkali-activated slag (AAS) with a 6% solution and 8M molarity at 28 days, as shown in Figure 8. In contrast, the minimum CS value of 5.1 MPa was noted for Type C AAS with a 4% solution and 6M molarity

at 7 days, as shown in Figure 6. The findings underscore the impact of the type of AAS, its concentration, and the molarity of NaOH on compressive strength. As molarity increases, compressive strength improves across all combinations, indicating enhanced geopolymerization with higher alkaline concentrations. A higher percentage of AAS correlates with increased CS, attributed to the enhanced availability of reactive silica and alumina that contribute to the formation of stronger geopolymeric bonds. Type B consistently demonstrates superior compressive strength compared to Types A and C, a result of utilizing distilled water in its formulation. Distilled water reduces impurities, thereby enhancing the efficiency of chemical reactions and improving matrix formation. The elevated compressive strength values of Type B at 8M molarity and increased AAS percentages are attributable to a more effective reaction between the activators and aluminosilicate materials, resulting in a denser and stronger polymeric structure [32]. Conversely, Type C exhibits comparatively lower CS values, particularly at reduced molarities and AAS percentages. The absence of sodium silicate ( $Na_2SiO_3$ ) likely accounts for the reduced silica content and diminished quality of the geopolymer matrix. The conventional cement mix demonstrates the lowest compressive strength values, as the geopolymer mechanism in alkali-activated slag-based mixes offers a more chemically bonded and compact structure in contrast to the hydration process in traditional cement. The relationship among AAS type, molarity, and percentage significantly affects compressive strength, with optimal activator conditions and effective polymerization leading to higher values [33].



Figure 7. CTM for Compressive Strength

Table 3. Compressive Strength for All Kinds of Blocks

No.	Type of Alkali Activator Solution	% of AAS	CS @ 7 Days (6M)	CS @ 14 Days (6M)	CS @ 28 Days (6M)	CS @ 7 Days (7M)	CS @ 14 Days (7M)	CS @ 28 Days (7M)	CS @ 7 Days (8M)	CS @ 14 Days (8M)	CS @ 28 Days (8M)
<b>Conventional Mix CS</b>			4.6	6.1	7.8	4.6	6.1	7.8	4.6	6.1	7.8
1	A	4	6.2	8.3	10.4	12.5	14.2	15.6	11.4	12.34	18.72
2	A	5	7.1	9.2	11.5	16.5	18.4	20	19.5	21.6	26.74
3	A	6	10.1	12.8	15.2	22.1	26.5	29.3	26.62	30.88	34.97
4	B	4	10.5	13.1	15.8	16.3	19.4	21.7	18.89	19.34	26.25
5	B	5	8.2	10.5	12.9	18.2	20.1	24.5	20.56	22.33	33.33
6	B	6	8.4	11.5	13.8	20.1	32.5	38	20.94	38.97	47.32
7	C	4	5.1	7.5	9.2	10.5	11.6	13.2	12.46	12.99	14.4
8	C	5	8.6	10.8	12.4	18.9	26.2	29.5	21.6	32.07	33.5
9	C	6	8.9	11.3	13.5	19.1	29.2	33.4	21.98	36.24	38.2

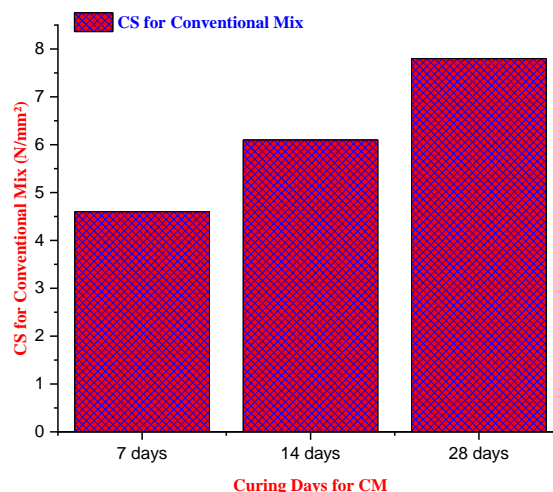


Figure 8. Compressive Strength for Conventional Mix

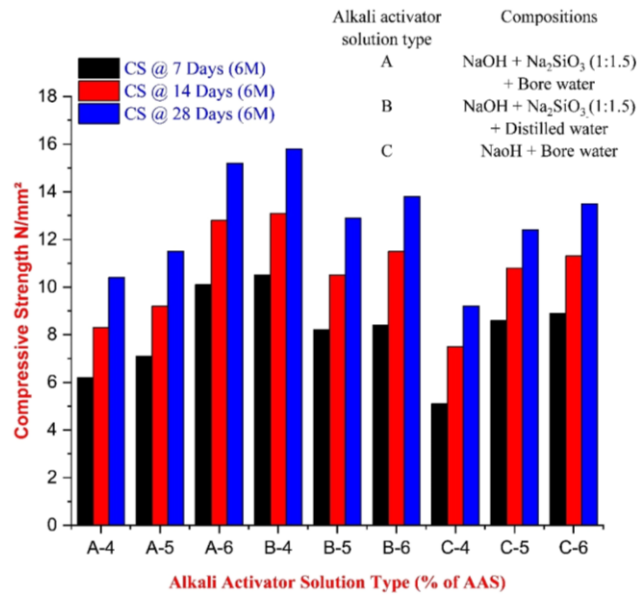


Figure 9. Compressive Strength for 6M NaOH

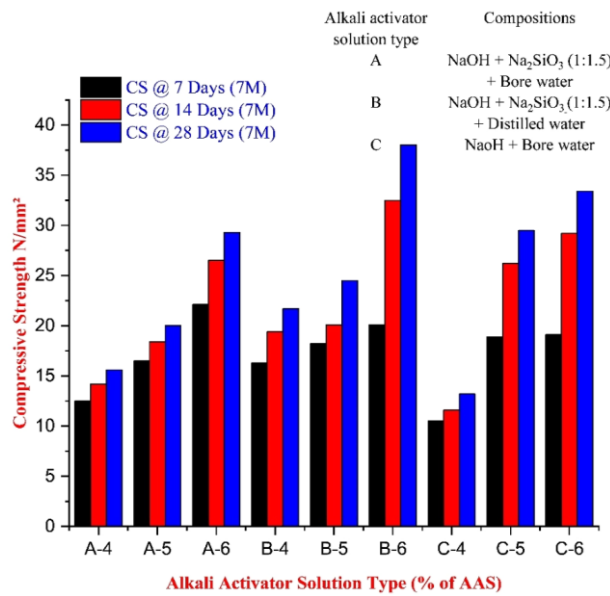


Figure 10. Compressive Strength for 7M NaOH

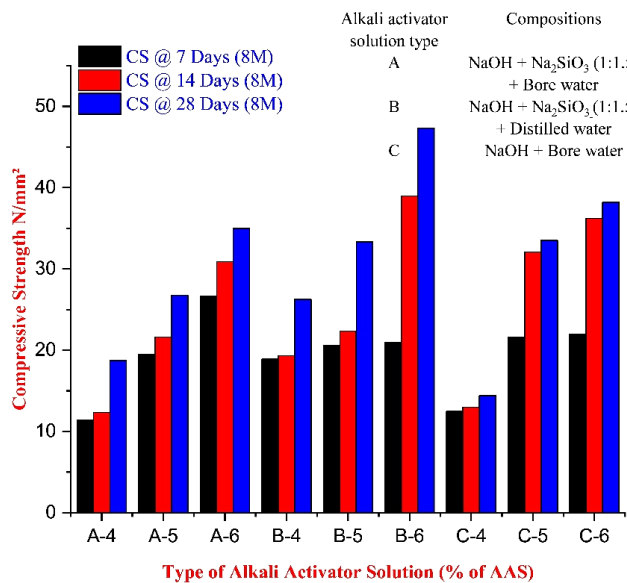


Figure 11. Compressive Strength for 8M NaOH

Figure 12 presents analyses conducted using Energy Dispersive X-ray Spectroscopy (EDS) on samples after compressive strength tests. Three regions, designated as (a), (b), and (c), illustrate the elemental composition of the material across various areas, accompanied by their respective weight percentages [34]. The dominant elements in the spectrum (a) are oxygen (59.3%), silicon (17.1%), and aluminium (10.9%), which indicate the formation of aluminosilicate and hydrated compounds that are essential for the geopolymer matrix. Trace elements such as calcium, sodium, and iron indicate partial geopolymerization, which contributes to moderate compressive strength. Spectrum (b) exhibits elevated levels of silicon (19.3%) and aluminium (13.8%) relative to (a), suggesting enhanced polymerization that results in improved matrix densification and increased strength. The sodium content of 2.3% facilitates alkali activation, whereas the trace levels of copper and zinc are likely derived from impurities or additives. Spectrum (c) demonstrates notable carbon content (14.8%) alongside reduced silicon (9.6%) and aluminium (7.3%) levels, suggesting incomplete geopolymerization. The high carbon content suggests the existence of unreacted carbonates or carbonaceous compounds, which may function as fillers but might also, weaken structure. The high salt content of 12.5% indicates that the reaction did not completely use the extra alkali. This area probably shows regions of insufficient reactivity that can create weaknesses, therefore affecting the compressive strength generally. The difference in element distribution across areas shows the degree of geopolymerization, therefore stressing the need for consistent mixing and curing to lower unreactive zones and enhance the general performance of the material [35].

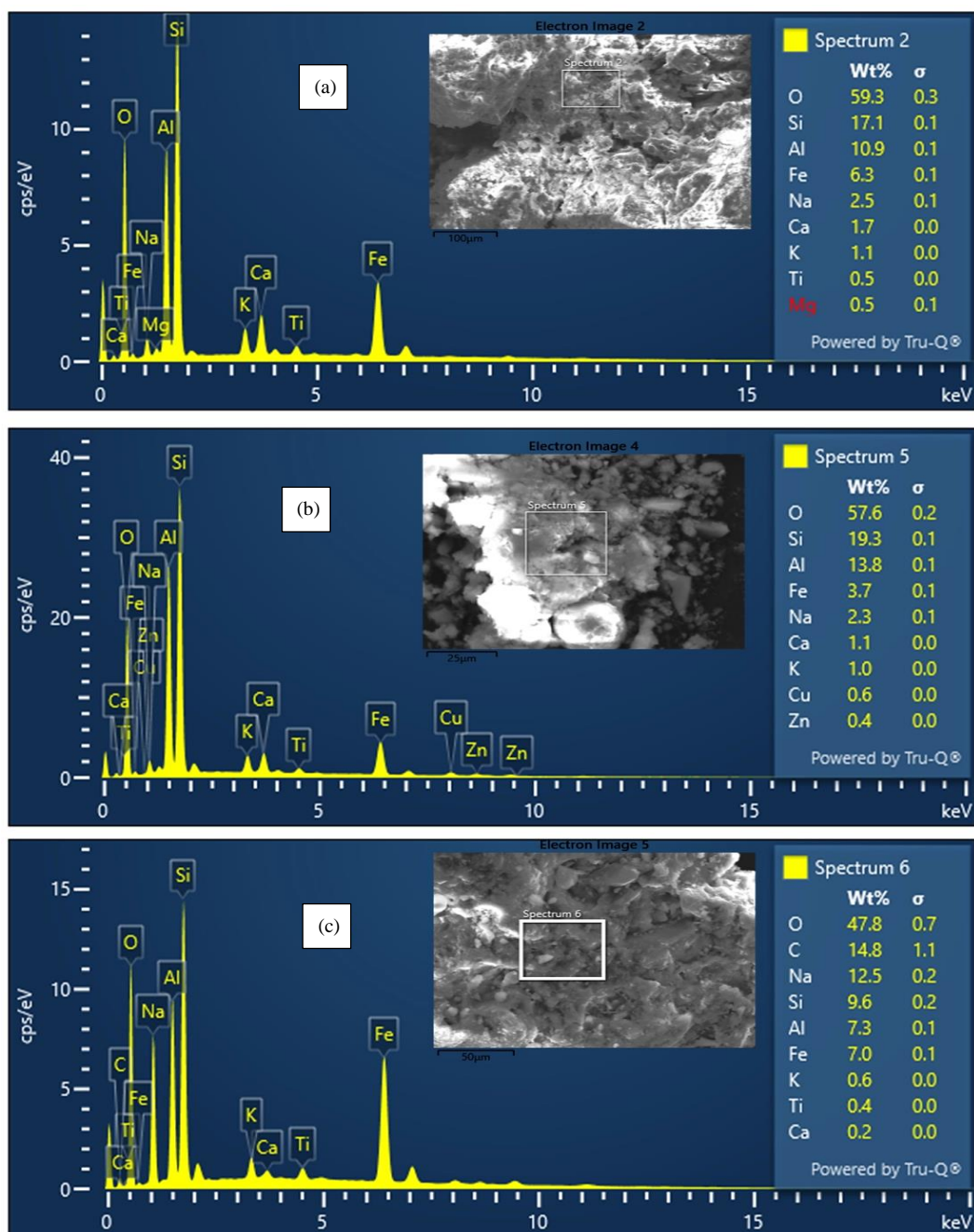


Figure 12. SEM and EDS of after-compressive strength (a) Sample B-6 (8M), (b) Sample C-6 (8M), and (c) Sample A-4 (8M)

**Prism Strength**

Figure 13 shows the Universal Testing Machine (UTM) used at the Saveetha School of Engineering (Chennai, India) laboratory for the prism test. The prism test evaluates masonry prism compressive strength, therefore mirroring the performance of masonry buildings under load. Understanding the interconnections and contributions of different masonry components—including blocks and mortar—to the general structural strength depends on this test. Using a uniaxial compressive load applied on the prism, important information on the load-bearing capacity and structural performance of the masonry results. The results help to evaluate material suitability for building and guide the design of constructions following durability and safety requirements. This work investigated the mechanical characteristics and structural dependability of brick prisms using different alkali activator solutions and molarities, therefore providing information on their compressive strength [36-38].



**Figure 13. UTM for Prism Test**

Table 4 shows masonry block prism strength under different percentages of Alkali Activator Solution (AAS), molarities (6M, 7M, and 8M), and curing times (7, 14, and 28 days). The results show that molarity, kind of AAS, and concentration used affect strength. Figures 14 to 16 show the prism strength depending on varied molarity and different samples. Type B had the greatest prism strength of 33.12 MPa; it showed 6% AAS and 8M molarity at 28 days, as indicated in Figure 16. By contrast, Type C showed the lowest strength of 4.8 MPa with 4% AAS and 6M molarity at 7 days, as displayed in Figure 14. This comparison emphasizes how much block strength is affected by AAS type, molarity, and curing time. Higher molarity—more especially, 8M—always results in higher prism strength across all AAS kinds and percentages. This is attributed to enhanced geopolymerization, resulting in a stronger and denser matrix formed through improved chemical reactions between alkali activators and aluminosilicate precursors. Type B consistently demonstrates superior performance compared to Types A and C, especially at elevated molarities. This is likely attributable to its effective combination of sodium hydroxide and sodium silicate with distilled water, which enhances geopolymerization and matrix densification. Type C, devoid of sodium silicate, typically demonstrates reduced strength due to the diminished formation of a strong polymeric network. The percentage of AAS is significant; higher percentages (6%) lead to increased prism strength owing to the enhanced availability of reactive materials that facilitate bond formation. The curing period enhances strength, as extended durations facilitate the complete reaction of alkali activators with precursors, minimizing unreacted phases and leading to a more robust matrix. The findings highlight the necessity of optimizing AAS composition, molarity, and curing duration to attain enhanced strength in masonry blocks.

**Table 4. Prism Strength for All Kinds of Blocks**

No.	Alkali Activator Solution Type	% of AAS	Prism Strength @ 7 Days (6M)	Prism Strength @ 14 Days (6M)	Prism Strength @ 28 Days (6M)	Prism Strength @ 7 Days (7M)	Prism Strength @ 14 Days (7M)	Prism Strength @ 28 Days (7M)	Prism Strength @ 7 Days (8M)	Prism Strength @ 14 Days (8M)	Prism Strength @ 28 Days (8M)
1	A	4	5.8	6.5	7.2	7.2	8.4	9.1	7.98	8.64	13.1
2	A	5	6.2	7.1	8.3	10.5	13.2	15.1	13.65	15.12	18.72
3	A	6	8.1	9.2	10.8	13.5	16.2	18.1	18.63	21.62	24.48
4	B	4	8	9.5	10.1	12.2	10.6	11.8	18.38	13.22	13.54
5	B	5	6.9	7.6	8.4	10.8	12.5	15.2	14.39	15.63	23.33
6	B	6	7.2	8.9	9.8	11.9	16.2	18.3	14.66	27.28	33.12
7	C	4	4.8	5.1	6.2	7.5	7.8	8.6	8.72	9.09	10.08
8	C	5	7.2	8.1	9.1	11.9	15.1	16.8	15.12	22.45	23.45
9	C	6	7.5	8.9	10	12.3	18.2	19.7	15.39	25.37	26.76

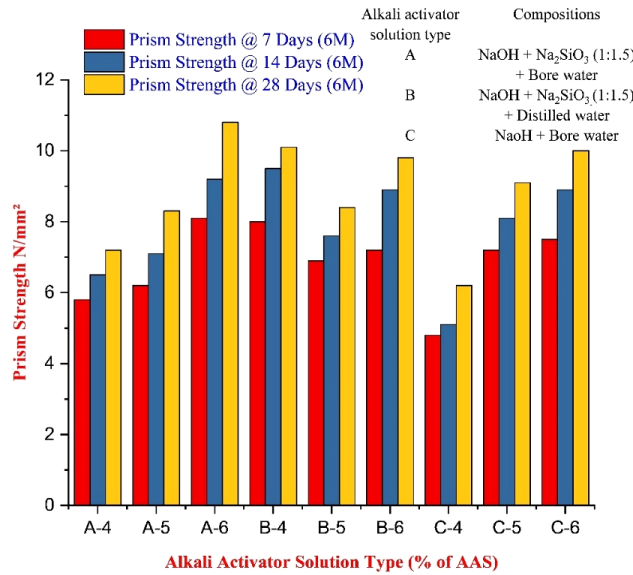


Figure 14. Compressive Strength for 6M NaOH

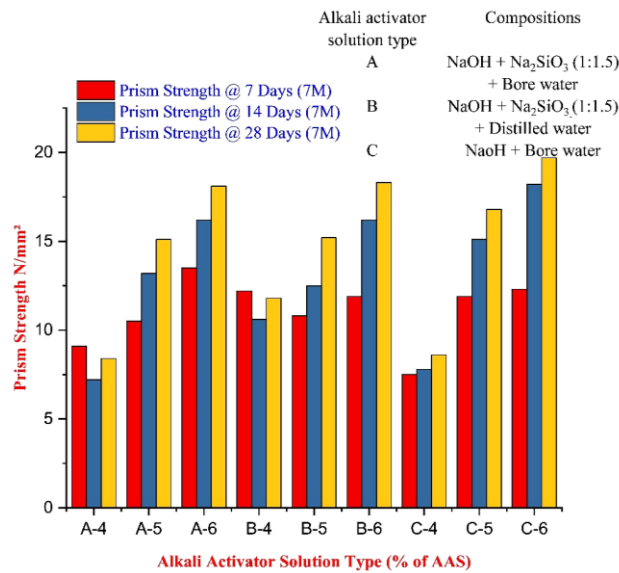


Figure 15. Compressive Strength for 7M NaOH

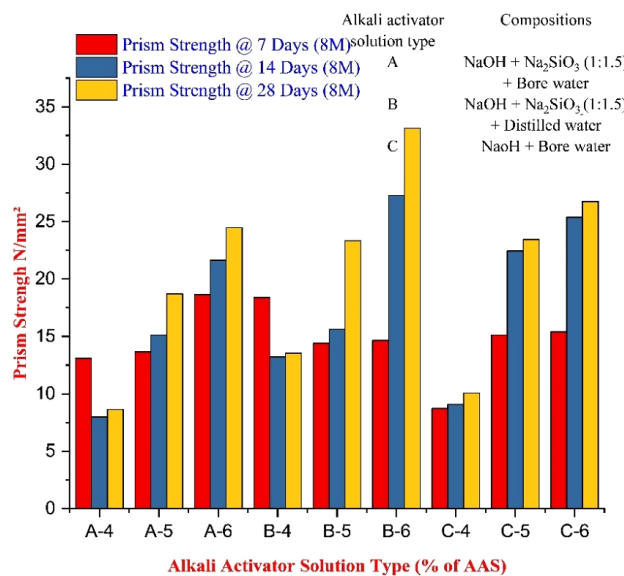


Figure 16. Compressive Strength for 8M NaOH

### Crack and Failure Pattern

In general, load masonry materials like bricks, fly ash bricks, and soil-stabilized blocks. When subjected to a compressive force, cracks will form due to the load from the compressive testing machine. The various types of failure are as follows: 1. Vertical Cracks (Splitting Failure) 2. Diagonal Cracks (Shear Failure) 3. Conical or Hourglass Failure 4. Corner and Edge Cracking 5. Explosive Brittle Failure.

Figure 17 shows the failure pattern of conventional SSB. Here in this block corner and edge cracking occurs, which was initiated at the edges and corners, leading to failure. Generally, SSB causes more failure since it does not contain AAM. Figure 18 shows the failure pattern of the 6MB6 sample. Here in this block shear failure occurs, and cracks form at approximately  $45^\circ$  from the vertical axis. The reason behind this crack is poor inter-particle bonding or excessive lateral expansion since these blocks are made of low geopolymer content. Figure 19 shows the failure pattern of the 7MB6 sample. Here in this block hourglass failure occurs, in which the top and bottom portions remain intact while the middle portion crushes inward. However, this block does not show more cracks since the AAM content used in this block is greater than 6MB6. Due to AAM content, Geopolymerization occurs, which makes the blocks stronger and denser. Figure 20 shows the failure pattern of the 8MB6 sample. Here in this sample, a mild vertical crack occurs even after achieving the highest compressive strength of  $47.32 \text{ N/mm}^2$ . It is concluded that the crack will not occur for the block that contains more AAM.



Figure 17. Crack and failure pattern for conventional block (SSB)



Figure 18. Crack and failure pattern for sample 6MB6



Figure 19. Crack and failure pattern for sample 7MB6



Figure 20. Crack and failure pattern for sample 8MB6

### 3.2. Durability Tests

Figure 21 presents the durability tests performed on masonry blocks to assess their resistance to different environmental and chemical conditions. The Water Absorption Test (A) evaluates the porosity of blocks by quantifying the volume of water absorbed upon submersion, which is essential for assessing their appropriateness in moisture-sensitive settings. The Chloride Test (B) assesses the resistance of blocks to chloride ion penetration, which is crucial for ensuring durability in coastal or industrial areas where exposure to chloride is common. The Acid Test (C) provides information on the blocks' performance in chemically demanding situations by assessing their ability to withstand acidic conditions. Particularly in areas with sulfate-rich soils or water, the sulfate Test (D) measures the resistance of blocks to sulphate assault, therefore influencing expansion and cracking. These tests evaluate, under different environmental and chemical exposures, the long-term structural dependability and durability of masonry blocks [23, 36-39].

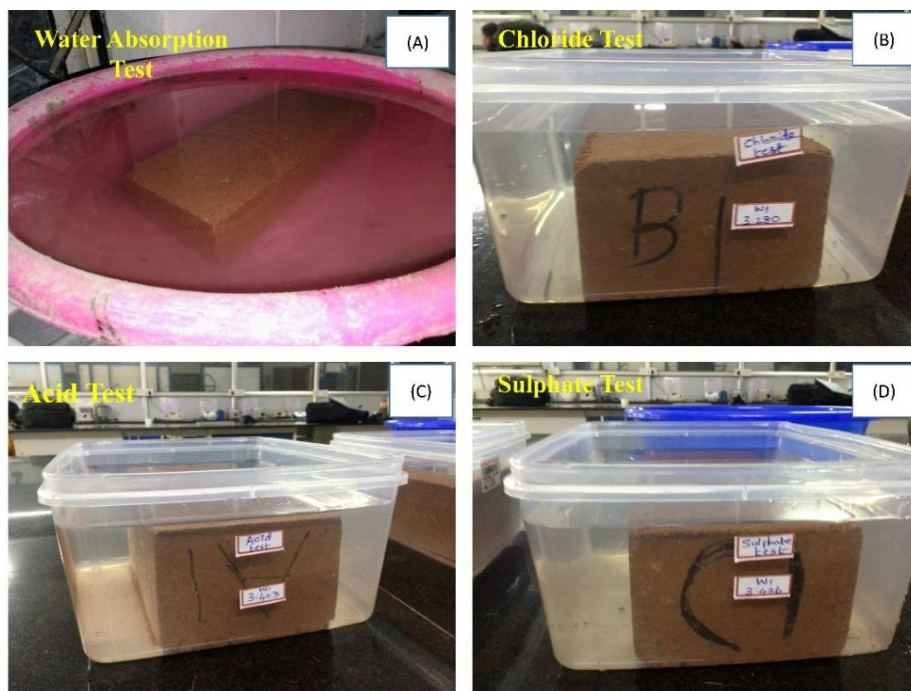


Figure 21. Durability tests

Using an 8M AAS concentration, Tables 5 to 8 show the results of multiple durability tests—including water absorption, chloride diffusion, acid diffusion, and sulphate diffusion—conducted on geopolymer masonry blocks (GMBs). Every test provides valuable information on the performance of many samples—more especially, those assigned A, B, and C—that have different percentages of Alkali Activator Solution (AAS). The results of the Water Absorption Test (Table 5) demonstrate that sample B6 (6% AAS) has the lowest water absorption at 5.20%, outperforming other samples, including C6 (10.33%) and A4 (8.15%). Reduced water absorption indicates lower porosity and enhanced durability. The enhanced performance of B6 results from an optimized binder composition that improves packing density and minimizes water ingress. In the Chloride Diffusion Test (Table 6), sample B6 exhibits the optimal performance, characterized by the lowest chloride diffusion rate of 1.87%. C6 exhibits the highest diffusion rate at 4.47%, suggesting a reduced capacity to resist chloride ion penetration. The decreased chloride diffusion in B6 can be attributed to its dense microstructure, which limits the pathways available for chloride ions to infiltrate. In the Acid Diffusion Test (Table 7), sample B6 exhibits the lowest acid diffusion at 3.33%, in contrast to A5 at 4.49% and C4 at

4.39%. This indicates the enhanced chemical resistance of B6, likely attributable to its stable matrix and diminished levels of unreacted materials, which may be susceptible to acid attack. In the Sulphate Diffusion Test (Table 8), sample B6 demonstrates the lowest diffusion rate at 1.05%, surpassing other samples, including A5 at 2.31% and C5 at 2.03%. The reduced sulphate diffusion in B6 demonstrates its superior resistance to sulphate-induced deterioration, a critical factor for blocks utilized in sulphate-rich environments. Sample B6 demonstrates consistently high performance across all tests, attributed to its superior binder matrix and dense microstructure. The balanced alkali activator composition and optimized mix design effectively reduce porosity, enhance chemical resistance, and minimize diffusion rates. B6 is therefore a suitable option for applications that demand high durability and resistance to environmental and chemical exposure.

**Table 5. Water absorption test for 8M Concentration Blocks**

No.	Alkali Activator Solution Type	% of AAS	Final Weight of GMB (Kg)	Initial Weight of GMB (Kg)	Water Absorption (%)
1	A	4	3.449	3.189	8.15
2	A	5	3.415	3.162	8.00
3	A	6	3.408	3.168	7.58
4	B	4	3.394	3.191	6.36
5	B	5	3.367	3.178	5.95
6	B	6	3.318	3.154	5.20
7	C	4	3.414	3.164	7.90
8	C	5	3.481	3.169	9.85
9	C	6	3.504	3.176	10.33

Figure 22 represents the water absorption percentage on the Y-axis, with sample types (A4, A5, A6, B4, B5, B6, C4, C5, & C6) displayed on the X-axis. Each bar represents a specific sample, with B6 indicating the lowest water absorption at 5.20%, and C6 indicating the highest at 10.33% [40].

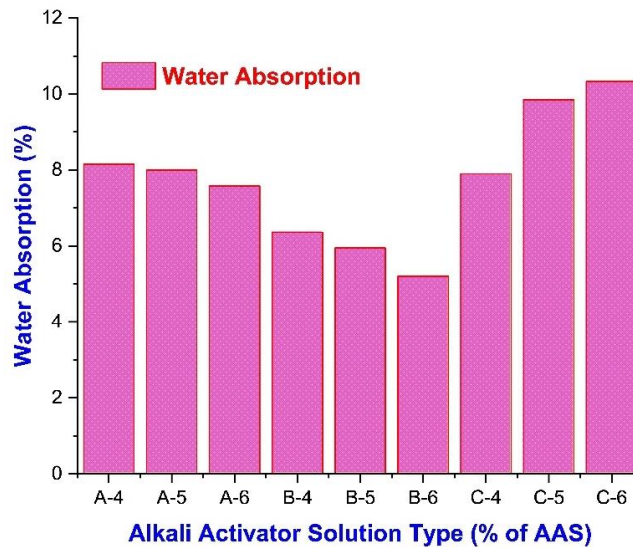


**Figure 22. Water absorption for 8M Concentration Blocks**

**Table 6. Chloride Diffusion test for 8M Concentration Blocks**

No.	Alkali Activator Solution Type	% of AAS	Initial Weight of GMB (kg)	Final Weight of GMB (kg)	Chloride Diffusion (%)
1	A	4	3.189	3.084	3.29%
2	A	5	3.162	3.062	3.16%
3	A	6	3.168	3.076	2.90%
4	B	4	3.191	3.097	2.95%
5	B	5	3.178	3.084	2.96%
6	B	6	3.154	3.095	1.87%
7	C	4	3.164	3.021	4.52%
8	C	5	3.169	3.045	3.91%
9	C	6	3.176	3.034	4.47%

Chloride Diffusion Test Figure 23 Representation of the diffusion percentage (Y-axis) for all samples (X-axis) in the context of chloride diffusion. The B6 sample exhibits the highest performance with the lowest diffusion percentage at 1.87%, whereas C4 and C6 demonstrate greater diffusion percentages, indicated by their taller bars [41].

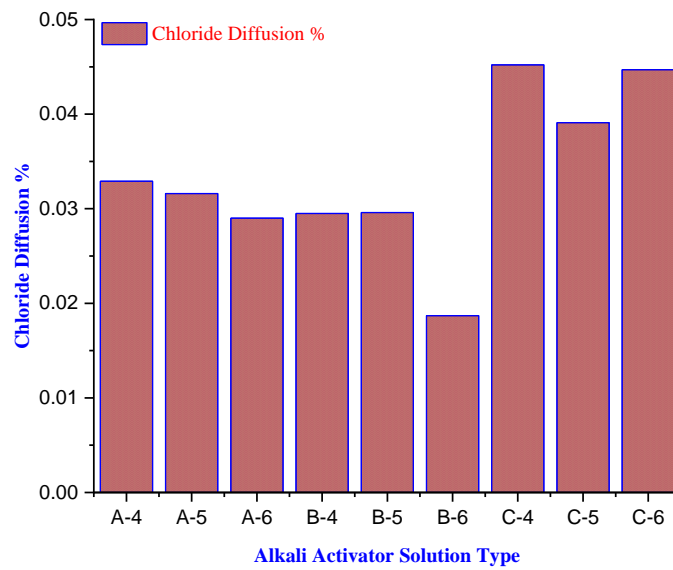


Figure 23. Chloride Diffusion for 8M Concentration Blocks

Table 7. Acid Diffusion test for 8M Concentration Blocks

No.	Alkali Activator Solution Type	% of AAS	Initial Weight of GMB (kg)	Final Weight of GMB (kg)	Acid Diffusion %
1	A	4	3.189	3.05	4.36%
2	A	5	3.162	3.02	4.49%
3	A	6	3.168	3.032	4.29%
4	B	4	3.191	3.06	4.10%
5	B	5	3.178	3.045	4.19%
6	B	6	3.154	3.049	3.33%
7	C	4	3.164	3.025	4.39%
8	C	5	3.169	3.032	4.33%
9	C	6	3.176	3.04	4.28%

Figure 24 depicts the percentages of acid diffusion that can be illustrated through a bar chart. The Y-axis will denote acid diffusion percentages, while the X-axis will enumerate the samples. B6 (3.33%) exhibits the shortest bar, whereas A5 (4.49%) and C4 (4.39%) demonstrate comparatively taller bars, reflecting their reduced resistance to acid attack.

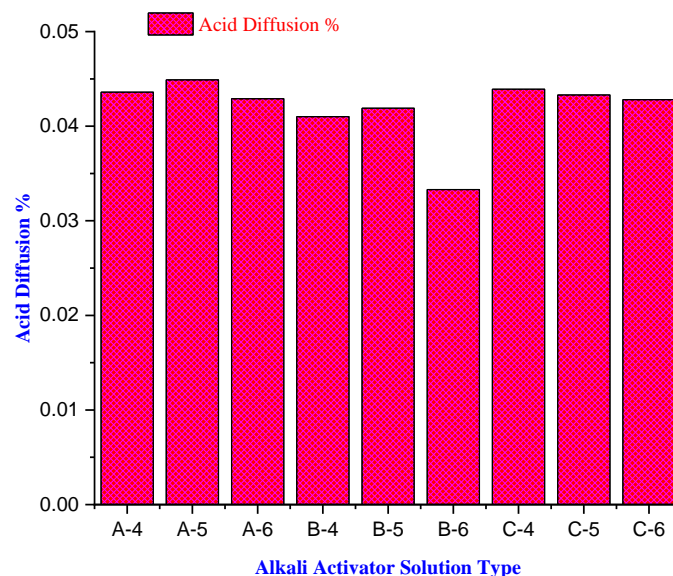
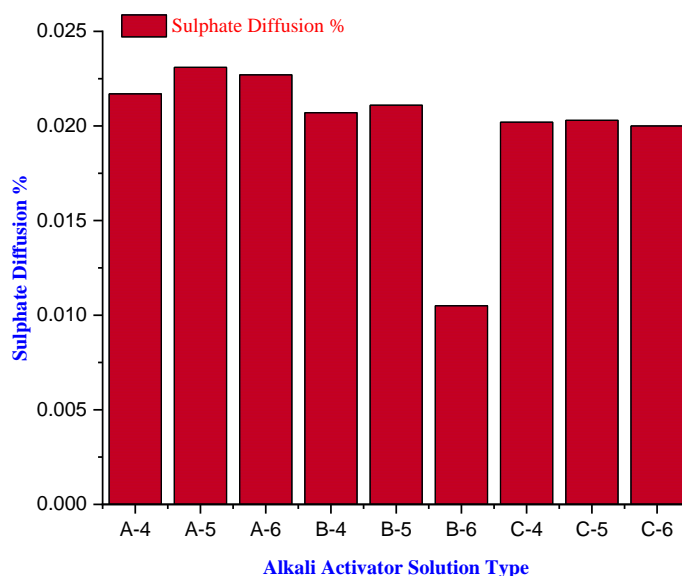


Figure 24. Acid Diffusion for 8M Concentration Blocks

**Table 8. Sulphate Diffusion test for 8M Concentration Blocks**

No.	Alkali Activator Solution Type	% of AAS	Initial Weight of GMB (kg)	Final Weight of GMB (kg)	Sulphate Diffusion %
1	A	4	3.189	3.12	2.17%
2	A	5	3.162	3.089	2.31%
3	A	6	3.168	3.096	2.27%
4	B	4	3.191	3.125	2.07%
5	B	5	3.178	3.111	2.11%
6	B	6	3.154	3.121	1.05%
7	C	4	3.164	3.118	2.02%
8	C	5	3.169	3.122	2.03%
9	C	6	3.176	3.13	2.00%

The sulphate diffusion percentages can be represented in Figure 25. The Y-axis will indicate the percentages of sulphate diffusion, whereas the X-axis will represent the samples. B6 (1.05%) exhibits the shortest bar, indicating superior performance, whereas A5 and A6 display taller bars, reflecting elevated diffusion rates. The B6 sample exhibits superior performance in multiple durability tests, including water absorption, chloride diffusion, acid diffusion, and sulphate diffusion, attributable to its optimal composition and densified microstructure. The low water absorption percentage of 5.20% signifies a compact structure characterized by a reduced number of pores, thereby decreasing water permeability. The precise ratio of alkali activator solution to binder enhances geopolymerization reactions, leading to a dense, impervious matrix. The B6 sample exhibits the lowest chloride diffusion percentage at 1.87%, indicating enhanced resistance to chloride penetration. The development of a denser network of alumino-silicate bonds minimizes pathways for chloride ions. The acid diffusion test indicates that the sample's performance (3.33%) surpasses that of others, demonstrating its resistance to chemical degradation. These phenomena are explained by the lowered porosity and chemical stability of the geopolymer matrix under acidic conditions. With the lowest result of 1.05%, the B6 sample shows outstanding performance in the sulphate diffusion test, therefore indicating strong resistance to sulphate assault. Including a 6% alkali activator and with a balanced composition produces stable hydration products that successfully fight sulphate intrusion. Conversely, samples exhibiting elevated diffusion and absorption values, such as C6 and A5, likely possess a greater degree of interconnected porosity and compromised microstructures, rendering them more vulnerable to degradation. The superior performance of the B6 sample is attributed to its balanced mix proportions and effective geopolymerization, leading to improved strength and durability.



**Figure 25. Sulphate Diffusion for 8M Concentration Blocks**

Table 9 illustrates the observed variation in compressive strength following durability tests is attributable to degradation mechanisms induced by chloride, acid, and sulphate environments. The initial compressive strength of each sample was maximal owing to the integrity of the material matrix. After exposure to aggressive environments, a progressive reduction in strength was observed in all samples, with the extent of loss varying according to the type of alkali activator solution and the diffusion test conducted. Sample A-6 exhibited a 6.72% decrease in strength following chloride diffusion (from 34.97 N/mm<sup>2</sup> to 32.62 N/mm<sup>2</sup>), which is less pronounced than the 28.76% decrease observed

after acid diffusion (from 34.97 N/mm<sup>2</sup>) to 27.64 N/mm<sup>2</sup>). Sample B-6 demonstrated notable resilience, maintaining 93.3% of its initial strength following chloride diffusion while decreasing to 71.3% after both acid and sulphate diffusion. The differing chemical interactions between the diffused agents and the binder matrix account for the varying impact, resulting in matrix dissolution, ion exchange, and microstructural weakening. This underscores the significance of material selection for durability under specific environmental conditions, as samples with stronger alkali activator solutions (e.g., A-6, B-6, C-6) demonstrated superior overall performance relative to their lower-strength counterparts (e.g., A-4, B-4, C-4) [42-44].

**Table 9. Compressive Strength after the Durability test**

No.	Alkali Activator Solution Type	Initial Strength (N/mm <sup>2</sup> )	After Chloride Diffusion (N/mm <sup>2</sup> )	After Acid Diffusion (N/mm <sup>2</sup> )	After Sulphate Diffusion (N/mm <sup>2</sup> )
1	A-4	12.34	11.51	9.76	8.81
2	A-5	26.74	24.96	21.17	19.1
3	A-6	34.97	32.62	27.64	24.92
4	B-4	19.34	18.05	15.3	13.8
5	B-5	33.33	31.1	26.37	23.78
6	B-6	47.32	44.15	37.42	33.76
7	C-4	14.4	13.44	11.39	10.27
8	C-5	33.5	31.25	26.5	23.9
9	C-6	38.2	35.63	30.21	27.26

Figure 26 illustrates the variations in compressive strength depicted in the graph following durability tests are affected by the interaction of alkali-activated materials with chloride, acid, and sulphate environments. The samples utilizing higher-strength alkali activator solutions, specifically A-6, B-6, and C-6, exhibited markedly increased compressive strength attributed to their denser and more durable matrices. Following exposure to chloride diffusion, a notable reduction in strength was observed. For instance, sample A-6 maintained 93.3% of its original strength, whereas lower-strength samples A-4 and B-4 exhibited more significant reductions attributed to weaker bonding and increased porosity, facilitating greater ion penetration. Acid diffusion resulted in a significant reduction in all samples, as it effectively dissolved binder materials and compromised the microstructure; for instance, B-6 exhibited a 21% decrease in strength, indicating its vulnerability to acid exposure. Sulphate diffusion resulted in considerable strength reductions in the majority of samples, frequently surpassing the losses attributed to acid diffusion. This results from the formation of expansive products such as ettringite, which generates internal stresses and contributes to the material's degradation. Samples with higher strength demonstrated superior resistance, maintaining greater strength than those with lower strength, underscoring the significance of material selection for durability in chemically aggressive settings.

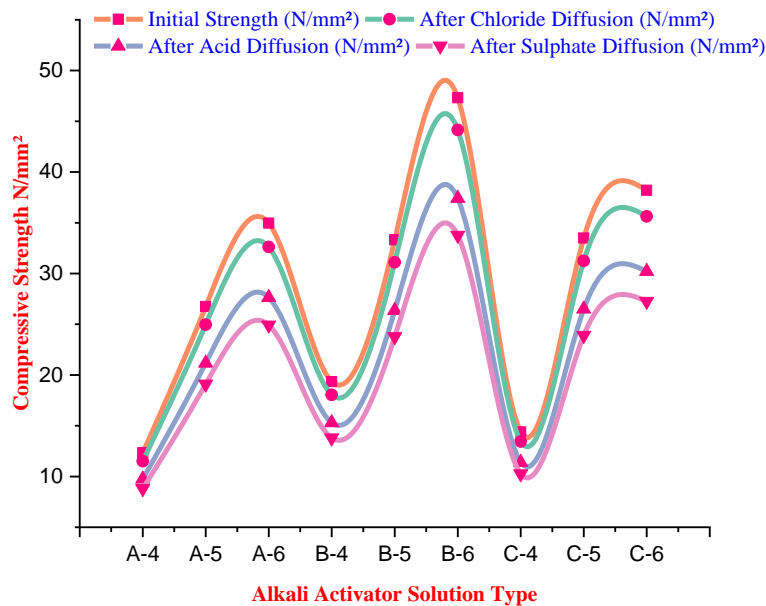


**Figure 26. Compressive Strength after Durability Test**

#### 4. Microstructure Analysis

Figure 27 illustrates the microstructural variations among samples prepared with different alkali activator solutions (8M-A4 to 8M-C6). The images illustrate the unique morphological features that affect the compressive strength and durability of the samples. - 8M-A4, 8M-B4, and 8M-C4 These samples demonstrate a porous structure characterized by loosely packed particles and observable voids. The elevated porosity and loosely bonded microstructure result in reduced initial compressive strength and heightened vulnerability to chloride, acid, and sulphate attacks. 8M-A5, 8M-B5, and 8M-C5. These images exhibit a denser matrix relative to their "4" counterparts, demonstrating improved interparticle bonding [34]. Reduced porosity enhances compressive strength and increases resistance to aggressive chemical environments. Nonetheless, minor voids and micro-cracks remain evident, potentially affecting long-term durability. 8M-A6, 8M-B6, and 8M-C6. These samples demonstrate the highest density in microstructure, characterized by minimal porosity and closely packed particles. The uniform bonding within the matrix results in the highest compressive strength among the samples and provides enhanced durability in chemical diffusion tests. The compact microstructure limits routes for chemical infiltration, thereby decreasing degradation rates. The transition from "4" to "6" in each series (A, B, and C) indicates a notable enhancement in microstructure density and particle bonding, which corresponds with improved compressive strength and chemical durability. This illustrates the significant influence of alkali activator concentration on the microstructural integrity and performance of geopolymer materials [45-47].

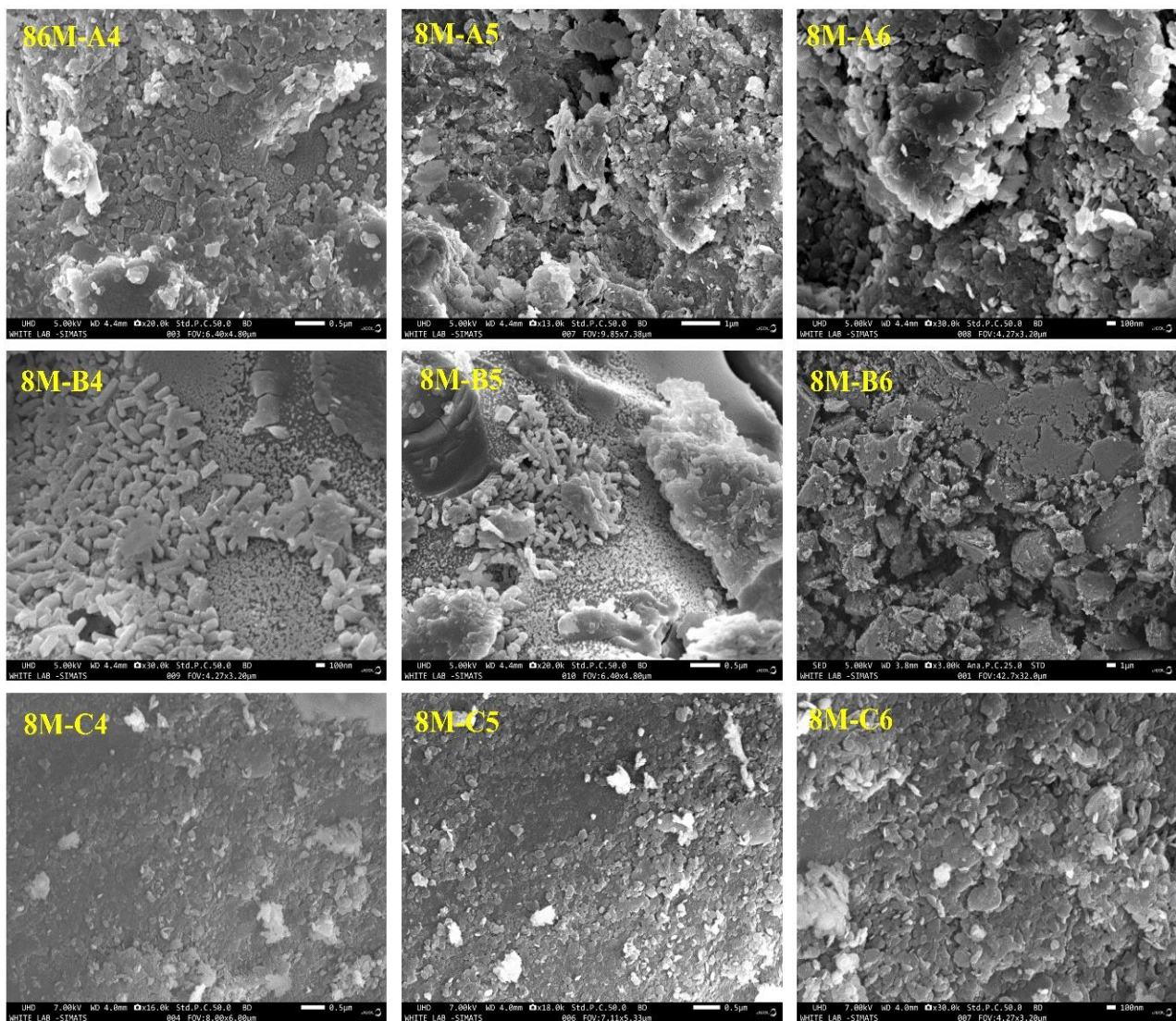


Figure 27. Microstructure analysis for 8M NaOH

The microstructural properties of geopolymer mud blocks, as observed through SEM, play a vital role in determining their compressive strength and durability. The SEM images of 8MB6, 8MC6, and 8MA6, which are shown in Figure 20, reveal distinct morphological differences that directly influence the mechanical performance of these blocks. The SEM image of 8MB6 likely exhibits a dense, compact microstructure with minimal porosity and well-developed geopolymer gel formation. The presence of a homogeneously distributed matrix with strong interparticle bonding enhances the load-bearing capacity, resulting in superior compressive strength and durability. The SEM image of 8MC6

shows a slightly higher degree of porosity or microcracks compared to 8MB6. While geopolymerization is well-developed, incomplete reaction phases or minor voids may contribute to a reduction in mechanical performance. The lesser strength compared to 8MB6 indicates the influence of microstructural defects on stress distribution and crack propagation. The SEM image of 8MA6 likely displays a more porous, loosely packed structure with visible unreacted particles and microcracks. Insufficient geopolymerization and weak interparticle bonding contribute to lower strength and reduced durability. Increased porosity accelerates moisture ingress, leading to potential degradation over time.

Durability is closely linked to microstructural integrity. A denser, well-bonded matrix (as in 8MB6) resists environmental degradation and maintains strength over extended periods. In contrast, higher porosity and microcracking (as seen in 8MA6) may lead to reduced resistance against water absorption, freeze-thaw cycles, and long-term mechanical stability. The study highlights the importance of microstructural optimization in geopolymer mud blocks. Enhancing particle packing, minimizing porosity, and promoting complete polymerization are essential for achieving superior mechanical properties and long-term durability. Future work should focus on refining processing conditions to mitigate defects and enhance block performance in practical applications. Compared with the existing results of previous studies, this experiment improved the compressive strength up to 36.05%. Its drastic improvement is changing the molarities in this study. The study does not increase more than 8M; the reason behind this is cost-effectiveness. If it increases the molarity, the cost of the study will increase. In that constrained limit, the study achieved more than 36 percent of compressive strength [12].

## 5. Conclusions

The research indicates that GMB serves as a sustainable and superior alternative to traditional SSB, providing improved strength, durability, and environmental advantages. The integration of locally sourced ASS and AAM at different molarity levels (6M, 7M, and 8M) and mix proportions (M1 to M3) resulted in enhanced performance of GMB.

- The compressive strength of the blocks exhibited an increase of 10–20% with the rise in molarity of the alkali solution from 6M to 8M. The M4 mix at 8M molarity demonstrated the highest compressive strength, exceeding 50 MPa, which corresponds to M50-grade concrete, thus rendering it appropriate for load-bearing walls in earthquake-resistant structures.
- Type B6 (6% AAS, 8M, 28 days) proved to be the most effective mixture, attaining a compressive strength of 47.32 MPa and a prism strength of 33.12 MPa. The material exhibited superior durability characteristics, with water absorption measured at 5.20%, chloride diffusion at 1.87%, acid diffusion at 3.33%, and sulphate diffusion at 1.05%. The application of distilled water and optimized binder content resulted in a dense matrix with minimal porosity, thereby significantly improving the mechanical and durability properties of the block. In contrast, Type C6 (6% AAS, 8M, 28 days) was determined to be the least effective mix, exhibiting high porosity, inadequate matrix quality, and unsatisfactory durability indicators, including water absorption (10.33%) and chloride diffusion (4.47%).
- The research indicated that GMB demonstrated greater resistance to acid, sulphate, and chloride attacks at elevated molarity levels, thereby improving their durability in harsh environments. Microstructural analyses corroborated these findings. XRD analysis confirmed the geopolymerization process by indicating changes in diffraction peaks. SEM images demonstrated denser microstructures at elevated molarity levels, which correlated with increased strength.
- The molarity levels were restricted to 6M, 7M, and 8M based on preliminary studies done in our research laboratory, which indicated that these concentrations provide optimal geopolymerization while maintaining workability and cost-effectiveness. Higher molarity levels were considered but not tested, as they may lead to excessive alkali content, increasing production costs and potentially compromising the durability and environmental sustainability of the blocks.
- Dynamic load tests were not performed in this study. However, the claim regarding the suitability of GMB for earthquake-resistant structures is based on their enhanced compressive strength, durability, and improved bonding characteristics compared to traditional SSB. Our future studies should include dynamic load testing, such as cyclic loading and shake table experiments, to evaluate the seismic performance of GMB and confirm their structural integrity under real-world earthquake conditions.
- Among all the mixes, the mix that contained Type B6 (6% AAS, 8M, 28 days) had better strength as well as durability properties than the remaining combinations.

The research concludes that GMB surpasses SSB in strength and durability while also fostering sustainable construction practices using locally available materials and a reduction in environmental impact. The enhanced performance of GMB, especially the Type B6 mix, positions them as a sustainable and effective choice for upcoming construction initiatives, particularly in areas with significant environmental and structural requirements.

## 6. Declarations

### 6.1. Author Contributions

Conceptualization, A.K. and B.R.; methodology, A.K.; software, K.S.; validation, A.K., B.R., and K.S.; formal analysis, M.A.K.; investigation, B.R.; resources, A.K.; data curation, K.S.; writing—original draft preparation, A.K.; writing—review and editing, K.S.; visualization, M.A.K.; supervision, B.R.; project administration, A.K.; funding acquisition, M.A.K. All authors have read and agreed to the published version of the manuscript.

### 6.2. Data Availability Statement

The data presented in this study are available in the article.

### 6.3. Funding

The authors received no financial support for the research, authorship, and/or publication of this article.

### 6.4. Conflicts of Interest

The authors declare no conflict of interest.

## 7. References

- [1] Venkatarama Reddy, B. V. (2012). Stabilised soil blocks for structural masonry in earth construction. *Modern Earth Buildings: Materials, Engineering, Constructions and Applications*, 324–363. doi:10.1533/9780857096166.3.324.
- [2] Kolay, P. K., Kumar, S., & Tiwari, D. (2013). Improvement of Bearing Capacity of Shallow Foundation on Geogrid Reinforced Silty Clay and Sand. *Journal of Construction Engineering*, 2013(1), 1–10. doi:10.1155/2013/293809.
- [3] Medjo Eko, R., Offa, E. D., Yatchoupou Ngatcha, T., & Seba Minsili, L. (2012). Potential of salvaged steel fibers for reinforcement of unfired earth blocks. *Construction and Building Materials*, 35, 340–346. doi:10.1016/j.conbuildmat.2011.11.050.
- [4] Midhin, M. A. K., & Wong, L. S. (2024). Investigating Mechanical Properties of Metakaolin-Based Geopolymer Concrete Optimized with Wastepaper Ash and Plastic Granules. *Civil Engineering Journal*, 10, 209–234. doi:10.28991/CEJ-SP2024-010-011.
- [5] Zhang, M. H., & Islam, J. (2012). Use of nano-silica to reduce setting time and increase early strength of concretes with high volumes of fly ash or slag. *Construction and Building Materials*, 29, 573–580. doi:10.1016/j.conbuildmat.2011.11.013.
- [6] Pacheco-Torgal, F., & Jalali, S. (2012). Earth construction: Lessons from the past for future eco-efficient construction. *Construction and Building Materials*, 29, 512–519. doi:10.1016/j.conbuildmat.2011.10.054.
- [7] Gavigan, D., Goggins, J., & McCabe, B. (2012). Strength and durability performance of stabilised soil block masonry units. *International Association for Bridge and Structural Engineering: IABSE Symposium Report*, 98(6), 34–41.
- [8] Kandasamy, A., & Rachel, P. P. (2025). Experimental Investigation of Novel Soil-Stabilized Blocks Using Lime and Cement. *Signals and Communication Technology: Vol. Part F76*, 875–881. doi:10.1007/978-3-031-68952-9\_113.
- [9] Islam, M. S., Elahi, T. E., Shahriar, A. R., & Mumtaz, N. (2020). Effectiveness of fly ash and cement for compressed stabilized earth block construction. *Construction and Building Materials*, 255, 119392. doi:10.1016/j.conbuildmat.2020.119392.
- [10] Lavie Arsène, M. I., Frédéric, C., & Nathalie, F. (2020). Improvement of lifetime of compressed earth blocks by adding limestone, sandstone and porphyry aggregates. *Journal of Building Engineering*, 29. doi:10.1016/j.job.2019.101155.
- [11] Rivera, J. F., Mejía de Gutiérrez, R., Ramirez-Benavides, S., & Orobio, A. (2020). Compressed and stabilized soil blocks with fly ash-based alkali-activated cements. *Construction and Building Materials*, 264, 120285. doi:10.1016/j.conbuildmat.2020.120285.
- [12] Vignesh, N. P., Mahendran, K., Arunachalam, N., & Ali, M. (2020). Effects of Industrial and Agricultural Wastes on Mud Blocks Using Geopolymer. *Advances in Civil Engineering*, 1054176. doi:10.1155/2020/1054176.
- [13] Kandasamy, A., Priya Rachel, P., Ramesh, B., Khazaleh, M. A. L., & Krishna Kumar, P. (2024). From Brown Earth to Green Bricks—A Critical Analysis of Stabilized Mud Blocks for Sustainable Construction. *Lecture Notes in Civil Engineering: Vol. 528 LNCE*, Springer Nature, Singapore. doi:10.1007/978-981-97-4844-0\_60.
- [14] Kandasamy, A., & Ramesh, B. (2025). GMB: A Comprehensive Review of Material Composition, Structural Properties, and Ecological Impacts. *Materials Science Forum*, 1144, 87–98. doi:10.4028/p-Elof10.
- [15] Wong, C. L., Mo, K. H., Alengaram, U. J., & Yap, S. P. (2020). Mechanical strength and permeation properties of high calcium fly ash-based geopolymer containing recycled brick powder. *Journal of Building Engineering*, 32(June), 101655. doi:10.1016/j.job.2020.101655.

- [16] Raavi, S. S. D., & Tripura, D. D. (2020). Predicting and evaluating the engineering properties of unstabilized and cement stabilized fibre reinforced rammed earth blocks. *Construction and Building Materials*, 262, 120845. doi:10.1016/j.conbuildmat.2020.120845.
- [17] Thennarasan Latha, A., Murugesan, B., & Skariah Thomas, B. (2023). Compressed earth block reinforced with sisal fiber and stabilized with cement: Manual compaction procedure and influence of addition on mechanical properties. *Materials Today: Proceedings*, 1-9. doi:10.1016/j.matpr.2023.04.373.
- [18] Qian, L. P., Ahmad, M. R., Lao, J. C., & Dai, J. G. (2023). Recycling of red mud and flue gas residues in geopolymer aggregates (GPA) for sustainable concrete. *Resources, Conservation and Recycling*, 191, 106893. doi:10.1016/j.resconrec.2023.106893.
- [19] Kiki, G., Nshimiyimana, P., Kouchadé, C., Messan, A., Houngan, A., & André, P. (2023). Physico-mechanical and durability performances of compressed earth blocks incorporating quackgrass straw: An alternative to fired clay. *Construction and Building Materials*, 403, 133064. doi:10.1016/j.conbuildmat.2023.133064.
- [20] Razeghi, H. R., Geranghadr, A., Safaee, F., Ghadir, P., & Javadi, A. A. (2024). Effect of CO<sub>2</sub> exposure on the mechanical strength of geopolymer-stabilized sandy soils. *Journal of Rock Mechanics and Geotechnical Engineering*, 16(2), 670–681. doi:10.1016/j.jrmge.2023.04.017.
- [21] Rivas-Aybar, D., John, M., & Biswas, W. (2023). Can the Hemp Industry Improve the Sustainability Performance of the Australian Construction Sector? *Buildings*, 13(6), 17. doi:10.3390/buildings13061504.
- [22] M S, R. (2020). Compressed Geopolymer Mud Blocks Testing and Production - A Review. *International Journal for Research in Applied Science and Engineering Technology*, 8(6), 2283–2288. doi:10.22214/ijraset.2020.6367.
- [23] Tripura, D. D., & Kasinikota, P. (2023). Axial load behavior of unreinforced and reinforced hollow interlocking compressed stabilized earth block masonry walls. *Construction and Building Materials*, 407(September), 133451. doi:10.1016/j.conbuildmat.2023.133451.
- [24] Zhou, T., Zhang, H., Zhang, Z., Zhang, L., & Tan, W. (2023). Investigation of intralayer and interlayer shear properties of stabilized rammed earth by direct shear tests. *Construction and Building Materials*, 367(January), 130320. doi:10.1016/j.conbuildmat.2023.130320.
- [25] Abedi, M., Hassanshahi, O., Rashiddel, A., Ashtari, H., Seddik Meddah, M., Dias, D., Arjomand, M. A., & Keong Choong, K. (2023). A sustainable cementitious composite reinforced with natural fibers: An experimental and numerical study. *Construction and Building Materials*, 378(September 2022), 131093. doi:10.1016/j.conbuildmat.2023.131093.
- [26] Kandasamy, A., & Rachel, P. P. (2023). An Experimental Evaluation of the Impact of Moulding Moisture Content on the Compressive Strength of Unstabilised Compressed Earth Blocks. *E3S Web of Conferences*, 387(04014), 1–12. doi:10.1051/e3sconf/202338704014.
- [27] Befikadu Zewudie, B. (2023). Experimental Study on the Production and Mechanical Behavior of Compressed Lime-Cement-Stabilized Interlock Soil Blocks. *Advances in Materials Science and Engineering*, 2023. doi:10.1155/2023/2933398.
- [28] Preethi, R. K., & Venkatarama Reddy, B. V. (2020). Experimental investigations on geopolymer stabilised compressed earth products. *Construction and Building Materials*, 257, 119563. doi:10.1016/j.conbuildmat.2020.119563.
- [29] Wang, Y., Liu, X., Tang, B., Li, Y., Zhang, W., & Xue, Y. (2021). Effect of Ca/(Si + Al) on red mud based eco-friendly revetment block: Microstructure, durability and environmental performance. *Construction and Building Materials*, 304(February), 124618. doi:10.1016/j.conbuildmat.2021.124618.
- [30] Kumar, S. (2015). The properties and performance of red mud-based geopolymeric masonry blocks. In *Eco-Efficient Masonry Bricks and Blocks*, 311-328. doi:10.1016/B978-1-78242-305-8.00014-0.
- [31] Singh, S., Aswath, M. U., & Ranganath, R. V. (2020). Performance assessment of bricks and prisms: Red mud based geopolymer composite. *Journal of Building Engineering*, 32(April), 101462. doi:10.1016/j.job.2020.101462.
- [32] Sudhir, M. R., Beulah, M., Sasha Rai, P., & Gayathri, G. (2021). A microstructure exploration and compressive strength determination of red mud bricks prepared using industrial wastes. *Materials Today: Proceedings*, 46, 163–169. doi:10.1016/j.matpr.2020.07.171.
- [33] Schlesinger, M. E., King, M. J., Sole, K. C., & Davenport, W. G. (2015). *Mud Stabilized Blocks Production and Use: Technical Manual*. United Nations Industrial Development Organisation, Vienna, Austria.
- [34] Sabari, K., Muniappan, A., Deepanraj, B., & Jinnah Sheik Mohamed, M. (2024). Advanced Mechanical Performance Optimization of Friction Stir Welded AZ31 Magnesium Alloy Using Artificial Neural Network and Grey Relational Analysis. *Surface Review and Letters*, 25501173. doi:10.1142/S0218625X25501173.
- [35] Samali, B., Dowling, D. M., & Li, J. (2008). Static and dynamic testing of adobe-mudbrick structures. *Australian Journal of Structural Engineering*, 8(2), 159–170. doi:10.1080/13287982.2008.11464995.

- [36] Morel, J. C., Pkla, A., & Walker, P. (2007). Compressive strength testing of compressed earth blocks. *Construction and Building Materials*, 21(2), 303–309. doi:10.1016/j.conbuildmat.2005.08.021.
- [37] Subramaniaprasad, C. K., Abraham, B. M., & Kunhanandan Nambiar, E. K. (2015). Influence of Embedded Waste-Plastic Fibers on the Improvement of the Tensile Strength of Stabilized Mud Masonry Blocks. *Journal of Materials in Civil Engineering*, 27(7), 1–7. doi:10.1061/(asce)mt.1943-5533.0001165.
- [38] Riza, F. V., Rahman, I. A., Mujahid, A., & Zaidi, A. (2010). A brief review of Compressed Stabilized Earth Brick (CSEB). *CSSR 2010 - 2010 International Conference on Science and Social Research*, 999–1004. doi:10.1109/CSSR.2010.5773936.
- [39] Hegde, A. (2017). Geocell reinforced foundation beds-past findings, present trends and future prospects: A state-of-the-art review. *Construction and Building Materials*, 154, 658–674. doi:10.1016/j.conbuildmat.2017.07.230.
- [40] Kuenzel, C., Li, L., Vandeperre, L., Boccaccini, A. R., & Cheeseman, C. R. (2014). Influence of sand on the mechanical properties of metakaolin geopolymers. *Construction and Building Materials*, 66, 442–446. doi:10.1016/j.conbuildmat.2014.05.058.
- [41] Cui, L., Xiang, T., Hu, B., Lv, Y., Rong, H., Liu, D., Zhang, S., Guo, M., Lv, Z., & Chen, D. (2024). Design of monolithic superhydrophobic concrete with excellent anti-corrosion and self-cleaning properties. *Colloids and Surfaces A: Physicochemical and Engineering Aspects*, 685(January), 133345. doi:10.1016/j.colsurfa.2024.133345.
- [42] Han, B., Wang, Y., Dong, S., Zhang, L., Ding, S., Yu, X., & Ou, J. (2015). Smart concretes and structures: A review. *Journal of Intelligent Material Systems and Structures*, 26(11), 1303–1345. doi:10.1177/1045389X15586452.
- [43] Calkins, M. (2009). *Materials for sustainable sites: a complete guide to the evaluation, selection, and use of sustainable construction materials*. *Choice Reviews Online*, 46(070), 46-3868. doi:10.5860/choice.46-3868.
- [44] Ahmad, H., Mahboubi, A., & Noorzad, A. (2020). Scale effect study on the modulus of subgrade reaction of geogrid-reinforced soil. *SN Applied Sciences*, 2(3), 1–22. doi:10.1007/s42452-020-2150-4.
- [45] Zain, H., Abdullah, M. M. A. B., Hussin, K., Ariffin, N., & Bayuaji, R. (2017). Review on Various Types of Geopolymer Materials with the Environmental Impact Assessment. *MATEC Web of Conferences*, 97. doi:10.1051/mateconf/20179701021.
- [46] Garshasbi, S., & Santamouris, M. (2019). Using advanced thermochromic technologies in the built environment: Recent development and potential to decrease the energy consumption and fight urban overheating. *Solar Energy Materials and Solar Cells*, 191, 21–32. doi:10.1016/j.solmat.2018.10.023.
- [47] Omar Sore, S., Messan, A., Prud'homme, E., Escadeillas, G., & Tsobnang, F. (2018). Stabilization of compressed earth blocks (CEBs) by geopolymer binder based on local materials from Burkina Faso. *Construction and Building Materials*, 165, 333–345. doi:10.1016/j.conbuildmat.2018.01.051.